Magnetic Resonance Imaging 63 (2019) 235–243

Contents lists available at ScienceDirect

Magnetic Resonance Imaging

journal homepage: www.elsevier.com/locate/mri

Original contribution

Three-dimensional high-resolution simultaneous quantitative mapping of the whole brain with 3D-QALAS: An accuracy and repeatability study

Shohei Fujita[a,b], Akifumi Hagiwara[a,*], Masaaki Hori[c], Marcel Warntjes[d,e], Koji Kamagata[a], Issei Fukunaga[a], Christina Andica[a], Tomoko Maekawa[a,b], Ryusuke Irie[a,b], Mariko Yoshida Takemura[a], Kanako Kunishima Kumamaru[a], Akihiko Wada[a], Michimasa Suzuki[a], Yutaka Ozaki[a], Osamu Abe[b], Shigeki Aoki[a]

[a] Department of Radiology, Juntendo University Hospital, Tokyo, Japan
[b] Department of Radiology, Graduate School of Medicine, The University of Tokyo, Tokyo, Japan
[c] Department of Radiology, Toho University Omori Medical Center, Tokyo, Japan
[d] SyntheticMR AB, Sweden
[e] Center for Medical Imaging Science and Visualization (CMIV), Sweden

ARTICLE INFO

Keywords:
Myelin
Proton density
Quantitative magnetic resonance imaging
Relaxation time
Relaxometry
Synthetic magnetic resonance imaging

ABSTRACT

Background: Previous methods for the quantification of brain tissue properties by magnetic resonance imaging were mainly based on two-dimensional acquisitions and were thus limited to a relatively low resolution in the slice direction compared to three-dimensional (3D) acquisitions. The 3D-quantification using an interleaved Look–Locker acquisition sequence with a T2 preparation pulse (3D-QALAS) sequence may allow for simultaneous acquisition of relaxometry parameters in high spatial resolution.

Purpose: To evaluate bias, linearity, and day-to-day repeatability of relaxometry parameters, as well as tissue fraction maps, acquired with 3D-QALAS.

Materials and methods: Scan–rescan test of the 3D-QALAS sequence was performed on a 1.5-T scanner with the International Society for Magnetic Resonance in Medicine/National institute of Standards and Technology system phantom and 10 healthy volunteers (7 male, 3 female; mean age, 23.2 ± 3.6 years). Simple linear regression analysis, Bland–Altman plots, and intrasubject coefficients of variation (CV) were used to assess the reliability of 3D-QALAS sequence-derived parameters. The T1, T2, proton density (PD), and myelin volume fraction (MVF) of *in vivo* brain regions were compared with values obtained using the multidynamic multi-echo sequence.

Results: In the phantom study, the T1, T2, and PD values measured by 3D-QALAS showed strong linearity with the reference values (R^2 = 0.998, 0.998, and 0.960 for T1, T2, and PD, respectively) and high repeatability (mean CV of 1.2%, 2.8%, and 2.9% for T1, T2, and PD, respectively). The T1, T2, PD, and MVF values of *in vivo* brain regions obtained with 3D-QALAS were highly consistent within subjects, with mean intrasubject CVs of 0.5%, 0.5%, 0.4%, and 1.6% for the T1, T2, PD, and MVF values, respectively.

Conclusion: 3D-QALAS enables reliable measurement of T1, T2, PD, and MVF values of the whole brain in high spatial resolution across a clinically-relevant dynamic range.

1. Introduction

Quantification of brain tissue properties using magnetic resonance imaging (MRI) has been widely used for the assessment of normal development [1,2], aging [3–5], and diseases [6–9]. Quantitative MRI approaches allow for more objective, repeatable, and reliable evaluation of the tissue than does conventional MRI, which only allows for assessment based on the arbitrary signal contrast between tissues. Despite their potential benefits, quantitative MR techniques, such as obtaining T1, T2, and proton density (PD) values of tissue, are not

Abbreviations: BPV, Brain parenchymal volume; CSF, Cerebrospinal fluid; CV, Coefficient of variation; GM, Gray matter; ICC, Intraclass correlation coefficient; LOA, Limits of agreement; MDME, Multidynamic multi-echo; MRI, Magnetic resonance imaging; MVF, Myelin volume fraction; NoN, Other intracranial material; PD, Proton density; SD, Standard deviation; VOI, Volume of interest; WM, White matter

* Corresponding author at: Department of Radiology, Juntendo University School of Medicine, 1-2-1, Hongo, Bunkyo-ku, Tokyo 113-8421, Japan.
E-mail address: a-hagiwara@juntendo.ac.jp (A. Hagiwara).

https://doi.org/10.1016/j.mri.2019.08.031
Received 9 June 2019; Received in revised form 19 August 2019; Accepted 19 August 2019

performed in routine clinical examination, likely due to the low resolution of conventional mapping methods.

Several quantitative multiparametric approaches have been proposed to obtain high spatial resolution maps of the brain [10–13]. One such method uses a multidynamic multi-echo (MDME) sequence, which enables simultaneous tissue relaxometry of T1 and T2 relaxation times and PD, providing quantitative maps that are inherently aligned [10,14–17]. Myelin volume fraction (MVF) in a voxel can also be estimated, based on the acquired T1, T2, and PD values, assuming four compartments in brain tissues [18,19]. The MDME sequence has been used for evaluation in various brain diseases, such as multiple sclerosis [20,21], brain infarctions [22], and meningitis [23].

The MDME sequence used for quantitative synthetic MRI was based on a multi-slice 2D acquisition, which provided a relatively low resolution in the slice direction compared with 3D acquisitions. Recently, 3D-quantification using an interleaved Look–Locker acquisition sequence with a T2 preparation pulse (3D-QALAS) sequence has been developed for simultaneous quantification of T1 and T2 in cardiac imaging and showed high accuracy and precision in the heart as well as in phantoms with various tissue properties [24,25]. A previous study showed that 3D-QALAS can be reliably used for measuring cortical thickness and subcortical volumes in most brain regions [26]. However, no study to date has investigated the reliability of MR property quantification based on 3D-QALAS in the brain.

Here, we propose the application of the 3D-QALAS sequence for simultaneous acquisition of relaxometry parameters at high spatial resolution in the brain. The purpose of this study was to evaluate bias, linearity, and day-to-day repeatability of relaxometry parameters (*i.e.*, T1, T2, and PD values) of the brain acquired with 3D-QALAS by (a) evaluating T1, T2, and PD values of the International Society for Magnetic Resonance in Medicine/National institute of Standards and Technology (ISMRM/NIST) MRI system phantom measured by 3D QALAS on different days and (b) evaluating T1, T2, PD, MVF, and tissue fraction maps of brain tissues *in vivo*.

2. Materials and methods

In phantom studies, the accuracy and repeatability of the T1, T2, and PD measurements were evaluated using an ISMRM/NIST system phantom containing spheres with standardized values [27,28]. Evaluation *in vivo* was performed with volunteers using volume of interest (VOI) analysis on T1, T2, PD, and MVF maps of the brain.

2.1. MR protocol

All scans were performed on a 1.5-T scanner (A patched R5.3.0 Ingenia, Philips Healthcare, Best, The Netherlands) with a 12-channel head coil. The 3D-QALAS sequence is based on multi-acquisition 3D gradient echo, with five acquisitions equally spaced in time, interleaved with a T2 preparation pulse and an inversion pulse. Briefly, the four acquisitions after the inversion pulse are used to determine the apparent T1* relaxation time approaching the saturated M0* magnetization. T1* and M0* must be corrected for the effect of the semi-continuous series of RF flip angles during the acquisition time to retrieve the actual T1 and M0. All M0 values are then scaled to PD such that 100% PD corresponds to the M0 of pure water. The T1 data curve is extrapolated to just prior to the T2-prep pulse. T2 relaxation is then found using the ratio of the signal intensity just prior and just after the T2-prep pulse. An internal trigger started each of the five acquisitions every 900 ms, amounting to a total cycle time of 4.5 s. Further details of the 3D-QALAS sequence have been provided by previous studies [24,25]. The substantial difference between our study and the previous cardiac 3D-QALAS studies involves the spatial and temporal resolution: imaging of the brain requires higher spatial resolution than that of the heart, but no breath hold is required. The voxel size in the cardiac study was 2 × 2 × 12 mm, while that in our study was 1.2 × 1.2 × 1.2 mm. In terms of volume, the voxel size used in our study was only 3.6% (1.728/48 mm^3) of that used in the cardiac study. With a longer acquisition time per beat and many more cycles, we obtained a higher resolution. Accordingly, the scan parameters of the 3D-QALAS were as follows: axial acquisition; TR/TE, 6.6/3.0 ms; inversion delay times 100, 1000, 1900, 2800 ms; T2-prep echo time 100 ms; field-of-view (FOV), 250 × 250 × 168 mm; matrix size, 208 × 208 × 140; section thickness, 1.20 mm; flip angle, 4°; receiver bandwidth, 230 Hz/pixel; acceleration factor = 1.7, averages, 2; acquisition time, 20 min 34 s. The scan parameters of the quantification of relaxation times and proton density by MDME [10] were as follows: axial acquisition; TR/TE1/TE2, 4000/22/99 ms; FOV, 230 × 230 mm; matrix size, 192 × 192; section thickness, 5 mm; flip angle, 90°; receiver bandwidth, 158.5 Hz/pixel; acceleration factor = 2, averages, 1; acquisition time, 5 min 29 s.

2.2. Phantom evaluation

The ISMRM/NIST system phantom (High Precision Devices, Inc., Boulder, Colorado, USA) consisted of multiple layers of sphere arrays that contain standardized T1 and T2 relaxation times and PD. T1 spheres consisted of different concentrations of $NiCl_2$ solutions, with T1 ranging from 24 to 2640 ms. T2 spheres consisted of different concentrations of $MnCl_2$ solutions, with T2 ranging from 8 to 1542 ms. PD spheres consisted of different concentrations of H_2O and D_2O, with PD ranging from 5 to 100% water. Reference values were measured by magnetic resonance spectroscopy at 20 °C and were provided by the Physical Measurement Laboratory at NIST [27,28]. Six T1 spheres and seven T2 spheres with T1 and T2 values within the clinically-relevant dynamic range (200–1400 ms and 50–400 ms, respectively) were evaluated in the study. All 14 PD spheres of the phantom were used. The outer and inner diameter of each sphere were 20 mm and 15 mm, respectively. The reference values of the spheres are shown in Table 1.

The NIST/ISMRM system phantom was scanned with the 3D-QALAS sequence seven times on different days over a 1-month period. The phantom was placed in position 30 min prior to each scan to reduce the effect of motion on measurements. T1, T2, and PD maps were generated using the SyMRI software (version 0.45.5) [29]. A spherical VOI with a 10-mm diameter was manually placed at the center of each sphere on the T1, T2, and PD maps, and the mean values were recorded using ITK-SNAP (version 3.6.0.).

2.3. Healthy volunteer evaluation

The local review board approved this study, and written informed consent was acquired from all participants. Ten healthy volunteers were included in this study (7 male, 3 female; mean age, 23.2 ± 3.6 [SD] years). None of the participants had a history of a major medical condition or neurological or psychiatric disorder. Two radiologists (A.H. and S.F.) blindly assessed all volunteer examinations and confirmed that none had structural abnormalities.

A scan–rescan test, as well as comparison with the 2D-MDME sequence results, was performed for each volunteer. A 2D-MDME sequence was performed once, and the 3D-QALAS sequence was performed twice (for scan–rescan) in the same session, for all volunteers. Between the scan–rescan of the 3D-QALAS sequence, the volunteers exited the scanner and were asked to rest for a few minutes T1, T2, PD, and MVF maps were generated using the SyMRI software [29] for the VOI analysis. We performed VOI analysis based on a previous study [14]. In brief, we created 16 VOIs: 8 of white matter (WM; frontal, parietal, temporal, and occipital WM; genu and splenium of the corpus callosum, internal capsules, and middle cerebellar peduncles) and 8 of gray matter (GM; frontal, parietal, temporal, and occipital GM; insula, caudate, putamen, and thalamus) VOIs in the Montreal Neurological Institute space [30–32]. VOIs of the left and right sides were combined for analysis, except for those of the splenium. For each VOI, the mean

Table 1
Mean values of 7-day measurements of T1 and T2 relaxation times and proton density (PD) and their coefficients of variation (CVs) of the International Society for Magnetic Resonance in Medicine/National institute of Standards and Technology system phantom. Reference values measured with magnetic resonance spectroscopy at 20 °C were provided by National institute of Standards and Technology.

	T1 (ms)			T2 (ms)			PD (%)		
Sphere no.	Reference	Mean ± SD	CV (%)	Reference	Mean ± SD	CV (%)	Reference	Mean ± SD	CV (%)
1	272.3	285 ± 2	0.6	43.84	42 ± 1	2.9	5	NA	NA
2	384.1	389 ± 4	1.1	62.82	61 ± 1	1.3	10	NA	NA
3	527	505 ± 5	0.9	89.52	89 ± 1	1.1	15	10.5 ± 0.4	3.5
4	751	683 ± 7	1.0	137	122 ± 1	1.0	20	14.4 ± 0.2	1.1
5	1027	934 ± 7	0.7	186.1	163 ± 3	1.8	25	16.5 ± 1.1	6.9
6	1432	1334 ± 34	2.6	258.4	212 ± 8	3.8	30	18.7 ± 0.6	3.4
7				428.3	365 ± 26	7.4	35	22.1 ± 0.5	2.1
8							40	27.2 ± 0.8	2.8
9							50	31.4 ± 0.5	1.5
10							60	38.1 ± 0.6	1.5
11							70	44.6 ± 0.5	1.1
12							80	63.5 ± 5.4	8.4
13							90	82.7 ± 1.2	1.5
14							100	89.0 ± 0.8	0.8

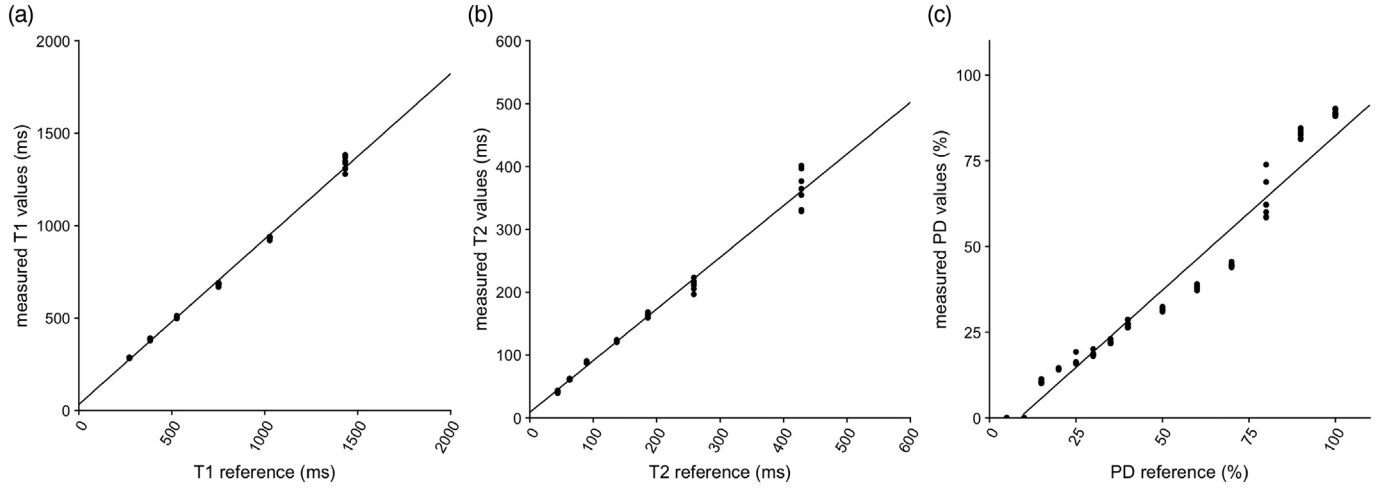

Fig. 1. Correlation plots comparing mean T1 (a), T2 (b), and PD (c) values to the reference values, showing linearity of measurements obtained with the 3D-QALAS sequence. Solid black lines represent the linear regression fit.

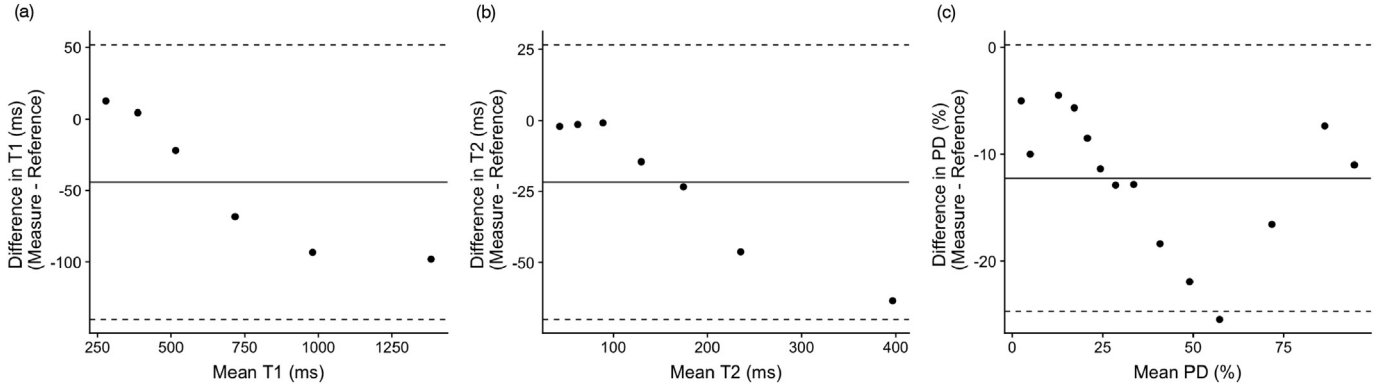

Fig. 2. Bland–Altman plots comparing T1 (a), T2 (b), and PD (c) values to the reference values, showing bias of measurements obtained with the 3D-QALAS sequence. The center solid lines represent mean differences. Upper and lower dotted lines represent the LOA, defined as the mean difference ± 1.96 × SD of the difference between the measurement and reference values. LOA, limit of agreement; SD, standard deviation.

T1, T2, PD, and MVF values were measured. *In vivo* repeatability and agreement with values obtained from MDME were evaluated for 3D-QALAS.

Based on the T1, T2, and PD values measured by the 3D-QALAS sequence, brain tissue segmentation was performed using the SyMRI software. The details of the brain segmentation algorithm using SyMRI are described elsewhere [19]. In brief, the measured quantitative values of brain tissues were used as coordinates in a 3D feature space (*i.e.*, R1–R2–PD space). This coordinate was referred to as a lookup grid, which shows the related partial tissue volumes to the 3D space [19]. We

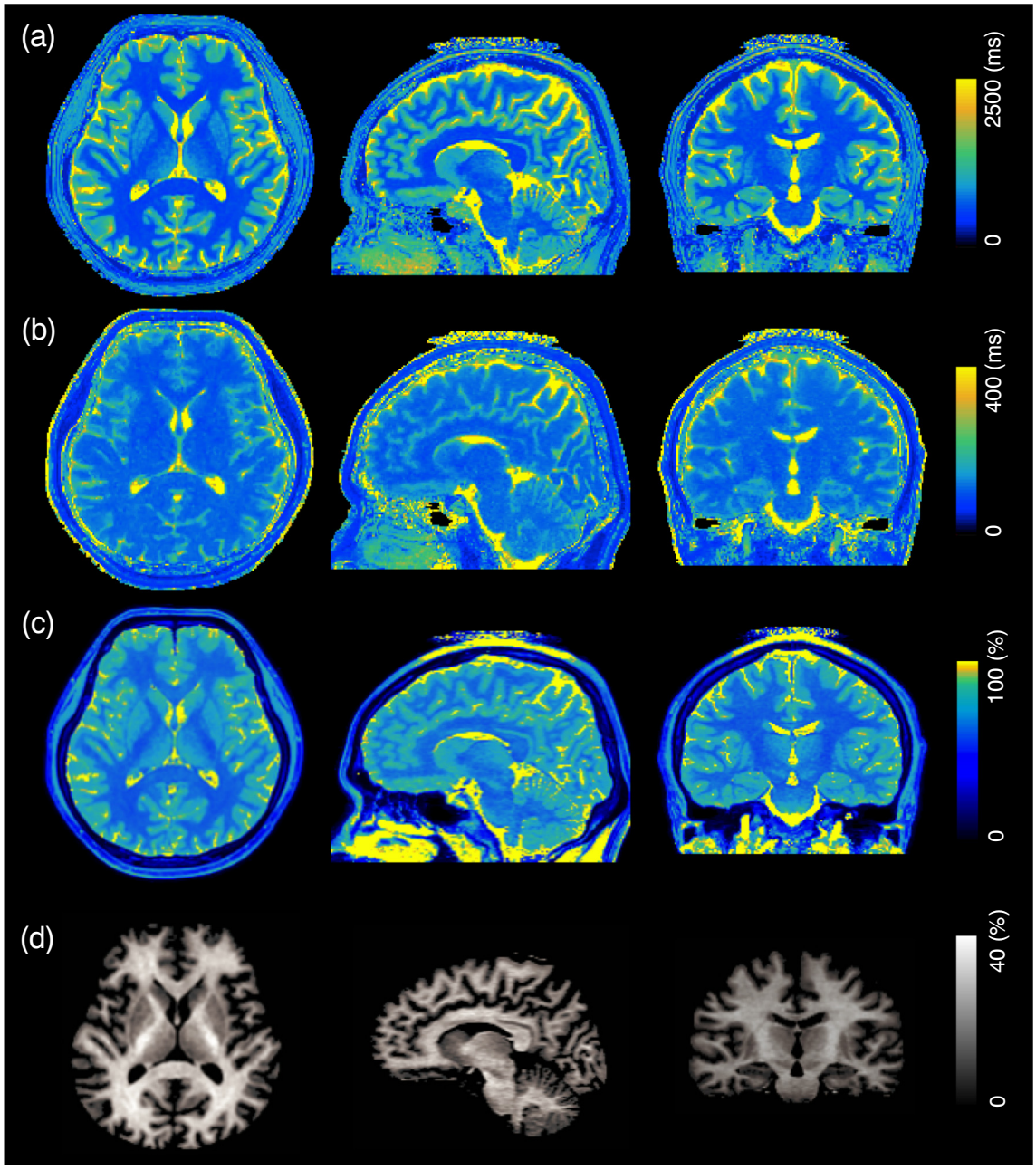

Fig. 3. Representative example of three-dimensional quantification maps of the brain. T1 maps (a), T2 maps (b), PD maps (c), and MVF maps (d) are shown in multiplanar reconstruction views. PD, proton density; MVF, myelin volume fraction.

performed brain tissue segmentation based on the same data to obtain GM, WM, and cerebrospinal fluid (CSF) volumes, and myelin volume (MYV) by multiplying the aggregated volume fraction of each tissue type in the whole brain and the voxel volume. Voxels not categorized as GM, WM, or CSF were classified as other intracranial material (NoN). The brain parenchymal volume (BPV) was calculated by summing the GM, WM, and NoN. The intracranial volume (ICV) was calculated by defining the borderline at PD = 50%. Agreement with volumes obtained from MDME and scan–rescan repeatability were evaluated for 3D-QALAS.

2.4. Statistical analysis

To assess linearity, simple linear regression analysis was performed between the mean of 7 measurements and the reference values that were provided by NIST [27,28]. For assessment of bias, Bland–Altman plots were obtained between the measurements and the reference values. The coefficients of variation (CVs) of the 7 measurements of the spheres in the phantoms was obtained to assess day-to-day repeatability. In the volunteer study, intrasubject CVs of T1, T2, and PD based on the scan–rescan tests were calculated for each VOI per subject (based on the scan–rescan tests) and then averaged across subjects. Percentage relative difference was used to assess reproducibility of the 3D-QALAS sequence-derived brain quantitative values and tissue volumes compared with those derived from MDME. For brain tissue volumes, intraclass correlation coefficients (ICCs) were also calculated to assess reproducibility.

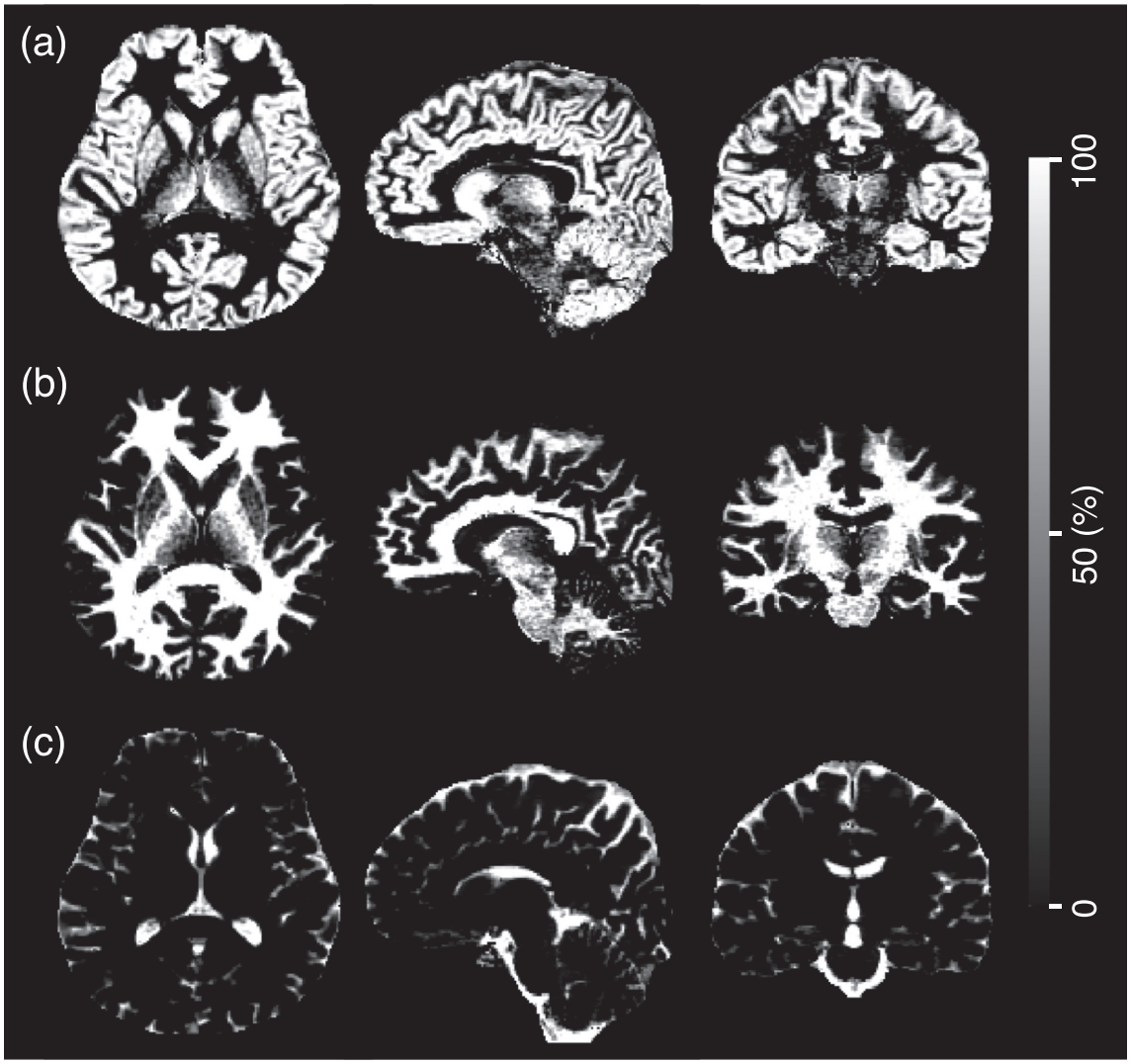

Fig. 4. Representative example of three-dimensional tissue fraction maps of the brain. GM (a), WM (b), and CSF (c) maps are shown in multi-planar reconstruction views. GM, gray matter; WM, white matter; CSF, cerebrospinal fluid.

3. Results

3.1. ISMRM/NIST MRI system phantom study

The temperature of the phantom after image acquisition was 19.1 ± 0.5 °C. The mean, SD, and CV of the repeated measurements of T1, T2, and PD of each sphere are reported in Table 1. All CVs of the T1, T2, and PD measurements based on 3D-QALAS were lower than 10% (mean CV: 1.2%, 2.8%, and 2.9%, respectively). Fig. 1 shows the simple linear regression analysis performed between the mean of the measurements and the reference values. The T1, T2, and PD values measured by 3D-QALAS all showed strong linearity with the reference values (R^2 = 0.998, 0.998, and 0.960, respectively). The linear regression fit had slopes of 0.89, 0.82, and 0.90, and intercepts of 33, 9.0, and −7.8 for T1, T2, and PD, respectively. Fig. 2 shows the Bland–Altman plots obtained between the measurements and the reference values; the difference between the measurements and reference values are plotted against the mean. The mean bias was −44 ms, −22 ms, and −12% for T1, T2, and PD, respectively. The limits of agreement (LOAs), defined as the mean difference ± 1.96 × SD of the difference between the measurements and reference values, were −140 to 51, −70 to 27, and −25 to 0.24 for T1, T2, and PD, respectively. All data points were within the LOAs, except for one data point of PD (reference value, 80% H_2O).

3.2. Heathy volunteer evaluation

Fig. 3 shows representative 3D T1, T2, PD, and MVF maps of the brain obtained from a healthy volunteer using 3D-QALAS. Fig. 4 illustrates tissue fraction maps obtained from a volunteer's scan. Fig. 5 shows a representative example of VOI placements in a multi-planar view.

Table 2 reports the mean, SD, and intrasubject CV of T1, T2, PD, and MVF values of each anatomic VOI across 10 healthy volunteers. Values obtained with the MDME sequence, and the relative difference between 3D-QALAS and MDME are also shown. Supplementary Table 1 shows the T1, T2, and PD values for representative anatomical parts of the brain obtained with 3D-QALAS along with values from the literature [10,11,33–38]. The T1, T2, PD, and MVF values of brain regions obtained with 3D-QALAS were highly consistent within volunteers, with mean intrasubject CVs of 0.5, 0.5, 0.4, and 1.6% for T1, T2, PD, and MVF, respectively. All *in vivo* measured values were within the dynamic range evaluated in the phantom study.

Table 3 reports the overall mean, intrasubject CV, ICC, and percentage relative difference of WM, GM, CSF, NoN, MYV, BPV, and ICV volumes based on 3D-QALAS and the 2D-MDME sequence for the 10 healthy volunteers. The WM, GM, MYV, BPV, and ICV values showed high agreement between the values obtained with 3D-QALAS and 2D-

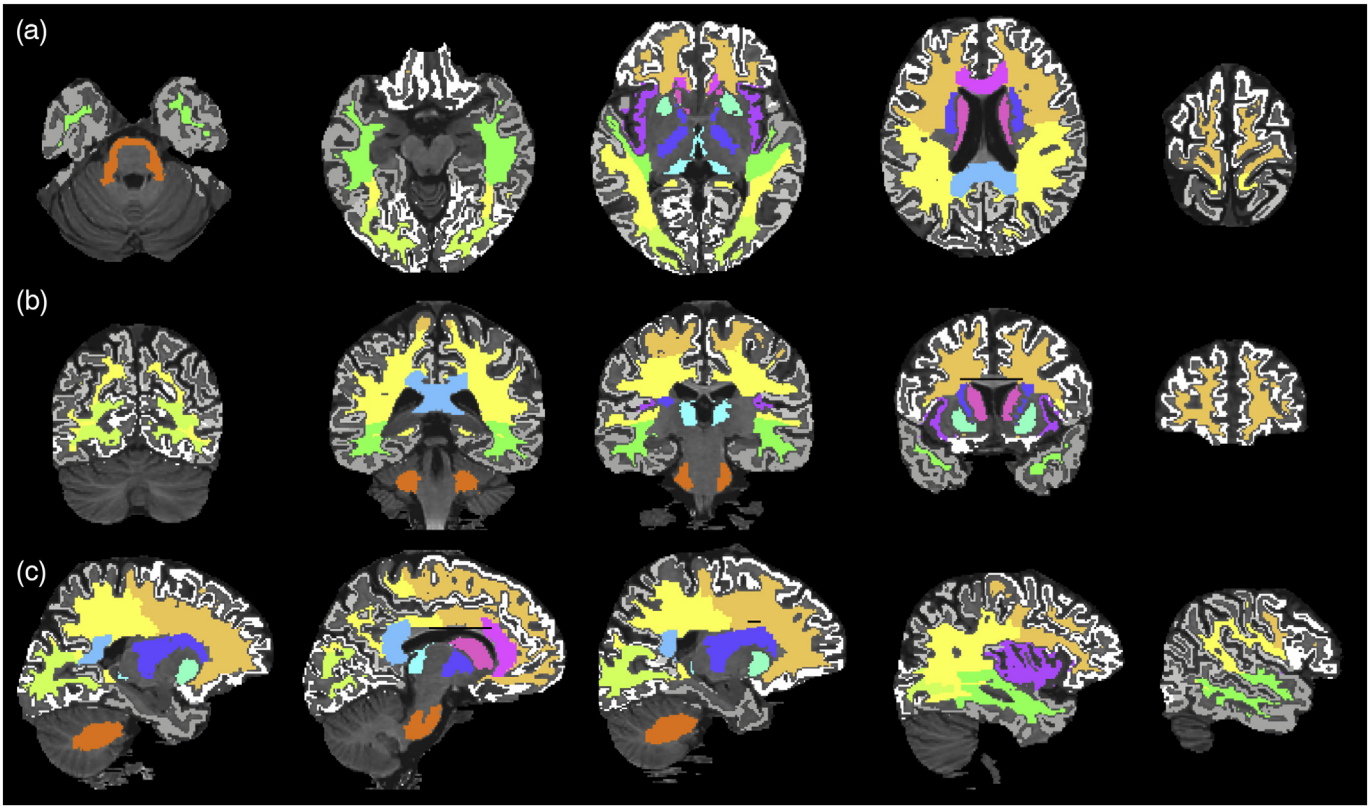

Fig. 5. Representative example of volume of interest (VOI) placement. VOIs are overlaid on a T1-weighed image in axial (a), coronal (b), and sagittal (c) views.

MDME, with percentage relative difference of 7.4%, 4.0%, 3.4%, 4.5%, and 1.3%, and ICCs of 0.97, 0.97, 0.95, 0.99, and 0.99, respectively. The CSF and NoN showed relatively low agreement between 3D-QALAS and 2D-MDME. The tissue volumes obtained with 3D-QALAS showed high repeatability, with a mean intrasubject CV of 1.9%.

4. Discussion

We presented the accuracy and repeatability of a relaxometry technique for 3D simultaneous quantification of T1, T2, PD, and MVF values of the whole brain. The T1, T2, and PD values obtained using the 3D-QALAS sequence showed high repeatability and strong linear correlation with the reference values of the standardized ISMRM/NIST system phantom. Although some biases were present with respect to the reference values, measurements were strongly linear, indicating that the 3D-QALAS sequence allows for adequate quantitative characterization. The T1, T2, and PD values of the healthy participants were in good agreement with the literature values, with high repeatability.

The 3D-QALAS sequence provides both quantitative values (*i.e.*, T1 and T2 relaxation times, PD, and MVF) and morphologic information of the whole brain in high spatial resolution. The method has the advantage that it can measure not only T1, T2, and PD values, but also MVF, which is considered to be important clinically. Another advantage of 3D-QALAS compared to other mapping techniques, which usually require multiple scans and registration, is that 3D-QALAS achieves perfect alignment among the obtained quantitative MR property maps and tissue fraction maps. Since the acquisition is performed slice-by-slice, only the effects of subject movement that occurred during the slice acquisition would be evident. The registration error should be eliminated, as long as the patient did not move during data acquisition within a slice.

Absolute quantification of MR properties using relaxometry has previously been reported to be useful for characterization of disease, assessment of disease activity, and monitoring of treatment [39–41]. The 3D isotropic acquisition with 3D-QALAS allows for generation of images from arbitrary views, without requiring additional scans from different directions. This property not only provides the advantage of visual characterization and detection of lesions, but also allows for accurate segmentation of small regional structures. This enables detecting and describing T1, T2, and PD changes within regional structures, which could be masked when averaging values over gross anatomic regions. Hence, 3D-QALAS has the potential to provide thorough and comprehensive characterization of brain lesions, as well as of the entire brain.

The validation of accuracy and repeatability of 3D-QALAS in a standardized phantom is a prerequisite for its clinical use. In our study, we compared the T1, T2, and PD values obtained using 3D-QALAS with the reference values in NIST/ISMRM phantoms across seven days. Day-to-day repeatability was lower than 3% for the T1, T2, and PD values. In the phantom study, we did not correct for temperature in T1 and T2 measurements. The correction would have lowered the reported CVs, because without the correction, the measurements would include error of the measurements and error originating from the temperature difference. However, in clinical practice, it is difficult and impractical to obtain the exact temperature of a subject. Because the CVs without temperature corrections were acceptable (mean CV of 1.2%, 2.8%, and 2.9%, for T1, T2, and PD, respectively) in our observation, we decided not to perform temperature correction.

The values acquired with 3D-QALAS showed a strong linear correlation (R^2 = 0.98–0.99) with the standardized values for the physiological range of structures of the brain. Our results indicate that 3D-QALAS covers the physiological range of T1, T2, and PD values in brain structures. PD values lower than 10% were estimated as 0%, suggesting that measurements of extremely low PD values would be less reliable. However, precise quantitative values of such tissues would be of less importance in the clinical setting; the PD values in the healthy human brain measured by MDME were reported to be 77% and 62% for GM and WM, respectively [14]. Further, PD values in various brain tumors

Table 2
Mean values and intrasubject coefficients of variation (CVs) of T1, T2, PD, and MVF for 10 healthy subjects, based on the 3D-QALAS sequence.

	T1 (ms)				T2 (ms)				PD (%)				MVF (%)			
	3D QALAS		MDME		3D QALAS		MDME		3D QALAS		MDME		3D QALAS		MDME	
Volume of interest	Overall mean (ms)	Intrasubject CV (%)	Overall mean (ms)	Relative difference (%)	Overall mean (ms)	Intrasubject CV (%)	Overall mean (ms)	Relative difference (%)	Overall mean (ms)	Intrasubject CV (%)	Overall mean (ms)	Relative difference (%)	Overall mean (ms)	Intrasubject CV (%)	Overall mean (ms)	Relative difference (%)
Gray matter																
Frontal GM	1044 ± 21	0.4 ± 0.3	1067 ± 29	1.9 ± 1.4	93 ± 2	0.9 ± 0.8	90 ± 2	4.2 ± 1.4	81 ± 0.7	0.4 ± 0.4	83 ± 1.1	2.2 ± 1.3	8.1 ± 0.7	2.9 ± 2.5	6.7 ± 0.7	15.6 ± 10.3
Parietal GM	1028 ± 22	0.6 ± 0.5	1068 ± 25	3.0 ± 1.3	90 ± 2	0.9 ± 0.7	87 ± 2	4.3 ± 1.0	79 ± 0.7	0.3 ± 0.1	83 ± 0.6	3.5 ± 0.7	8.8 ± 0.8	3.0 ± 2.2	6.0 ± 0.4	34.9 ± 6.1
Temporal GM	1092 ± 17	0.3 ± 0.3	1123 ± 31	2.6 ± 1.8	96 ± 2	0.5 ± 0.2	90 ± 2	5.8 ± 1.8	83 ± 0.5	0.4 ± 0.3	85 ± 0.6	2.6 ± 1.0	6.5 ± 0.5	1.2 ± 1.0	5.3 ± 0.5	19.2 ± 6.4
Occipital GM	1035 ± 22	0.6 ± 0.5	1079 ± 25	3.5 ± 1.0	87 ± 1	0.5 ± 0.4	85 ± 1	2.6 ± 1.1	80 ± 0.7	0.3 ± 0.2	83 ± 0.7	2.6 ± 0.6	8.3 ± 0.8	3.5 ± 1.6	6.7 ± 0.6	18.5 ± 7.8
Insular cortex	1048 ± 21	0.3 ± 0.2	1065 ± 29	1.3 ± 1.2	96 ± 2	0.4 ± 0.5	93 ± 2	4.0 ± 2.4	79 ± 0.5	0.3 ± 0.3	83 ± 0.8	4.8 ± 1.1	8.8 ± 1.0	0.8 ± 0.8	5.8 ± 0.8	35.9 ± 8.3
Caudate	918 ± 17	0.6 ± 0.5	878 ± 28	5.3 ± 2.0	85 ± 2	0.5 ± 0.4	82 ± 1	4.1 ± 1.6	77 ± 1.1	0.4 ± 0.4	79 ± 1.4	2.4 ± 1.4	12.4 ± 1.3	2.9 ± 2.8	10.1 ± 1.9	21.5 ± 15.1
Putamen	831 ± 15	0.7 ± 0.6	795 ± 22	5.3 ± 2.0	77 ± 2	0.6 ± 0.6	75 ± 2	2.3 ± 1.3	75 ± 0.5	0.3 ± 0.2	77 ± 0.6	2.1 ± 0.8	16.5 ± 0.9	1.6 ± 1.4	13.7 ± 0.8	16.7 ± 6.1
Thalamus	780 ± 13	0.5 ± 0.3	763 ± 20	2.9 ± 1.4	81 ± 1	0.4 ± 0.3	79 ± 1	2.3 ± 1.4	73 ± 0.5	0.3 ± 0.2	73 ± 0.7	0.6 ± 0.5	19.4 ± 0.6	1.1 ± 1.0	19.8 ± 1.1	4.7 ± 2.6
Aggregate of GM	910 ± 20	0.4 ± 0.3	904 ± 18	1.6 ± 1.0	88 ± 1	0.5 ± 0.5	83 ± 1	5.8 ± 0.8	77 ± 0.7	0.3 ± 0.3	77 ± 0.7	0.9 ± 0.4	14.1 ± 0.9	1.2 ± 1.0	15.2 ± 0.6	9.4 ± 4.8
White matter																
Frontal WM	581 ± 20	0.7 ± 0.4	615 ± 15	4.4 ± 1.2	76 ± 2	0.6 ± 0.6	76 ± 1	1.0 ± 0.6	65 ± 0.4	0.3 ± 0.2	63 ± 0.9	2.6 ± 0.9	31.1 ± 0.6	1.0 ± 0.7	33.9 ± 1.3	8.2 ± 2.5
Parietal WM	575 ± 20	0.3 ± 0.3	625 ± 16	7.2 ± 1.2	79 ± 1	0.4 ± 0.5	77 ± 1	2.4 ± 0.8	64 ± 0.3	0.2 ± 0.1	64 ± 0.8	0.7 ± 0.6	32.3 ± 0.5	0.6 ± 0.4	33.2 ± 1.2	2.3 ± 2.0
Temporal WM	599 ± 20	0.7 ± 0.6	637 ± 20	5.3 ± 1.3	78 ± 2	0.6 ± 0.7	76 ± 1	2.5 ± 1.3	66 ± 0.8	0.5 ± 0.4	65 ± 1.1	2.4 ± 1.0	28.9 ± 1.1	1.5 ± 1.4	31.6 ± 1.7	9.2 ± 2.9
Occipital WM	587 ± 20	0.7 ± 0.4	667 ± 12	11.9 ± 1.2	81 ± 1	0.4 ± 0.4	79 ± 1	3.2 ± 1.0	65 ± 0.7	0.4 ± 0.2	66 ± 0.6	1.5 ± 0.7	31.1 ± 1.0	1.0 ± 0.6	30.1 ± 1.0	3.7 ± 1.9
Genu of the CC	530 ± 18	0.5 ± 0.4	539 ± 16	1.0 ± 0.9	73 ± 2	0.8 ± 0.8	75 ± 1	2.3 ± 1.4	66 ± 1.5	0.5 ± 0.4	58 ± 1.2	11.4 ± 2.4	29.0 ± 2.3	1.5 ± 1.2	41.3 ± 1.8	29.7 ± 5.8
Splenium of the CC	540 ± 17	0.2 ± 0.2	584 ± 16	6.6 ± 1.8	79 ± 1	0.4 ± 0.5	78 ± 1	2.6 ± 1.8	65 ± 0.8	0.6 ± 0.4	61 ± 0.8	5.7 ± 2.3	30.8 ± 1.1	1.4 ± 1.0	36.9 ± 1.2	16.4 ± 5.8
Internal capsule	580 ± 21	0.6 ± 0.6	615 ± 19	4.5 ± 1.6	76 ± 2	0.7 ± 0.6	75 ± 1	2.2 ± 0.9	64 ± 0.7	0.3 ± 0.3	63 ± 0.9	1.1 ± 0.8	33.0 ± 1.0	0.9 ± 0.8	34.1 ± 1.4	3.7 ± 2.3
Middle cerebellar peduncle	631 ± 16	0.3 ± 0.3	684 ± 22	7.5 ± 1.8	83 ± 1	0.3 ± 0.2	81 ± 2	2.1 ± 1.3	67 ± 0.9	0.4 ± 0.3	66 ± 0.9	2.0 ± 0.9	28.0 ± 1.2	1.3 ± 1.1	29.9 ± 1.3	7.4 ± 3.0
Aggregate of WM	580 ± 19	0.4 ± 0.3	624 ± 14	6.1 ± 1.1	78 ± 1	0.4 ± 0.6	77 ± 1	1.8 ± 0.7	65 ± 0.4	0.3 ± 0.2	64 ± 0.8	1.7 ± 0.8	31.1 ± 0.5	0.8 ± 0.5	33.2 ± 1.2	6.0 ± 2.3

GM, gray matter; WM, white matter; CC, corpus callosum; MVF, myelin volume fraction.

Table 3
Volumetric measurements of healthy volunteers based on the 3D-QALAS sequence.

	3D QALAS		MDME		
Tissue type	Overall mean (ml)	Intrasubject CV	Overall mean (ml)	Relative difference (%)	ICC
WM	618 ± 64	0.8 ± 0.7	572 ± 59	7.4 ± 2.3	0.97
GM	722 ± 75	0.7 ± 0.7	694 ± 65	4.0 ± 2.4	0.97
CSF	137 ± 35	2.0 ± 1.4	212 ± 52	43.6 ± 5.4	0.93
NoN	39 ± 6	8.2 ± 5.9	50 ± 14	33.7 ± 18.6	0.04
MYV	197 ± 23	0.8 ± 0.8	199 ± 23	3.4 ± 1.5	0.95
BPV	1378 ± 128	0.5 ± 0.4	1317 ± 131	4.5 ± 1.0	0.99
ICV	1515 ± 151	0.4 ± 0.3	1529 ± 163	1.3 ± 0.6	0.99

MDME, multidynamic multi-echo; GM, gray matter; WM, white matter; CSF, cerebrospinal fluid; NoN, other brain material; BPV, brain parenchymal volume; ICV, intracranial volume; MYV, myelin volume; ICC, intraclass correlation coefficient.

have been previously reported by Just et al., who showed that tumors have higher PD values than does WM [42].

The T1, T2, and PD values obtained with 3D-QALAS showed good overall agreement with MDME sequence-derived values, as shown by relative differences. However, the MVF values in gray matter regions differed substantially between 3D-QALAS and MDME. One possible reason may be the low absolute value of MVF in gray matter (mean MVF value of 15.2% in gray matter compared to 33.2% in white matter), which may have made the relative differences sensitive to small changes. Despite the high absolute value of the MVF in the corpus callosum, values obtained with 3D-QALAS and MDME differed substantially. One possible reason for this could be the effects of incomplete elimination of B1 inhomogeneity and coil sensitivity, because the corpus callosum is located in the center of the field-of-view that is likely to be affected by these effects. Special attention is required when applying 3D-QALAS to the corpus callosum. In spite of these discrepancies, 3D-QALAS sequence-derived T1, T2, PD, and MVF values showed high repeatability. The measured values often differ even among well-established methods and pursuing the true value may be impractical for clinical use. When performing an examination in a clinical context to monitor subtle changes in subjects' MR values, repeatability is more important than accuracy, as repeatability is associated with the smallest change that can be detected using the measurement. As long as the measurement is consistent and shows high repeatability, it could be used to depict the differences among tissues.

The 3D-QALAS sequence was constructed for analyzing brain tissue and may not be suitable for quantifying MR properties of materials that differ greatly from the brain. Our data show that 3D-QALAS slightly underestimates the values of T1, T2, and PD. However, the repeatability of these measurements was high (mean CV of 1.2%, 2.8%, and 2.9% for T1, T2, and PD values, respectively), indicating that 3D-QALAS is suitable for longitudinal studies.

We also assessed the *in vivo* repeatability of 3D-QALAS with 10 healthy volunteers. The T1, T2, and PD values acquired with 3D-QALAS showed good agreement with the results of previous studies reporting values of structures of the normal brain at 1.5 T (Supplementary Table 1) [10,11,33–38]. The CVs of T1, T2, and PD values in volunteer data were lower than those measured in the phantom study. This may be because the size of the VOIs used in the phantom study was smaller than those used in the volunteer study. The tissue volume based on 3D-QALAS showed low intrasubject CV, lower than 1%, except for NoN. NoN showed intrasubject CVs of 8.2%, which was much higher than that of the other tissue volumes. Because the CV is sensitive to small changes when the mean value used as the denominator approaches zero, the small absolute volume of NoN may have contributed to the relatively large intrasubject CV.

This study had several limitations. First, the scanning time in this study was relatively long in terms of incorporation into a routine clinical scan. Using a 3-T MRI scanner, as well as combining it with acceleration techniques, such as compressed sensing [43], may reduce scan times to a clinically-applicable level. Second, only healthy volunteers and no patients were enrolled in the *in vivo* study. Although our goal was to validate the accuracy and repeatability of 3D-QALAS, future studies focusing on patients are required. Third, although we have validated the reliability of 3D-QALAS using the standardized phantom with reference values, the *in vivo* values were not compared with those acquired by gold-standard methods, such as IR-based T1 mapping and multi-echo T2 mapping, which requires an excessive scan time. However, the T1, T2, and PD values acquired with 3D-QALAS showed good agreement with values obtained with the well-established MDME sequence, as well as with values reported previously.

In conclusion, the three-dimensional relaxometry method, 3D-QALAS, allows for reliable measurement of T1, T2, and PD values across a clinically-relevant dynamic range, with high spatial resolution, while concurrently providing morphological information of the whole brain.

Supplementary data to this article can be found online at https://doi.org/10.1016/j.mri.2019.08.031.

Grant support

This work was supported by JSPS KAKENHI grant number 19K17177, 19K17150, 18K07692, 16K10327, and JP16H06280; Grant-in-Aid for Scientific Research on Innovative Areas- Resource and technical support platforms for promoting research ‘Advanced Bioimaging Support’; the Budget for promotion of strategic international standardization given by the Ministry of Economy, Industry, and Trade (METI); the Japan Agency for Medical Research and Development (AMED) under grant number 18lk1010025s0101 and 19lk1010025h9902; Brain/MINDS Beyond program from AMED under Grant Number JP19dm0307024h002; and the Japanese Society for Magnetic Resonance in Medicine.

Declaration of competing interest

Marcel Warntjes is currently employed part-time at SyntheticMR and has a stock in SyntheticMR.

Acknowledgements

We gratefully appreciate the cooperation of Ukihide Tateishi (Tokyo Medical and Dental University), the chair of Japan Quantitative Imaging Biomarkers Alliance (J-QIBA), and other J-QIBA members.

References

[1] Giedd JN, Snell JW, Lange N, Rajapakse JC, Casey BJ, Kozuch PL, et al. Quantitative magnetic resonance imaging of human brain development: ages 4-18. Cereb Cortex 1996;6(4):551–60.
[2] Grossman R, Hoffman C, Mardor Y, Biegon A. Quantitative MRI measurements of human fetal brain development in utero. Neuroimage 2006;33(2):463–70.
[3] Kumar R, Delshad S, Woo MA, Macey PM, Harper RM. Age-related regional brain

T2-relaxation changes in healthy adults. J Magn Reson Imaging 2012;35(2):300–8.
[4] Callaghan MF, Freund P, Draganski B, Anderson E, Cappelletti M, Chowdhury R, et al. Widespread age-related differences in the human brain microstructure revealed by quantitative magnetic resonance imaging. Neurobiol Aging 2014;35(8):1862–72.
[5] Carey D, Caprini F, Allen M, Lutti A, Weiskopf N, Rees G, et al. Quantitative MRI provides markers of intra-, inter-regional, and age-related differences in young adult cortical microstructure. Neuroimage 2018;182:429–40.
[6] Bottomley PA, Hardy CJ, Argersinger RE, Allen-Moore G. A review of 1H nuclear magnetic resonance relaxation in pathology: are T1 and T2 diagnostic? Med Phys 1987;14(1):1–37.
[7] Manfredonia F, Ciccarelli O, Khaleeli Z, Tozer DJ, Sastre-Garriga J, Miller DH, et al. Normal-appearing brain t1 relaxation time predicts disability in early primary progressive multiple sclerosis. Arch Neurol 2007;64(3):411–5.
[8] Jackson GD, Connelly A, Duncan JS, Grunewald RA, Gadian DG. Detection of hippocampal pathology in intractable partial epilepsy: increased sensitivity with quantitative magnetic resonance T2 relaxometry. Neurology 1993;43(9):1793–9.
[9] House MJ, St Pierre TG, Foster JK, Martins RN, Clarnette R. Quantitative MR imaging R2 relaxometry in elderly participants reporting memory loss. AJNR Am J Neuroradiol 2006;27(2):430–9.
[10] Warntjes JB, Leinhard OD, West J, Lundberg P. Rapid magnetic resonance quantification on the brain: optimization for clinical usage. Magn Reson Med 2008;60(2):320–9.
[11] Deoni SC, Peters TM, Rutt BK. High-resolution T1 and T2 mapping of the brain in a clinically acceptable time with DESPOT1 and DESPOT2. Magn Reson Med 2005;53(1):237–41.
[12] Ehses P, Seiberlich N, Ma D, Breuer FA, Jakob PM, Griswold MA, et al. IR TrueFISP with a golden-ratio-based radial readout: fast quantification of T1, T2, and proton density. Magn Reson Med 2013;69(1):71–81.
[13] Ma D, Gulani V, Seiberlich N, Liu K, Sunshine JL, Duerk JL, et al. Magnetic resonance fingerprinting. Nature 2013;495(7440):187–92.
[14] Hagiwara A, Hori M, Cohen-Adad J, Nakazawa M, Suzuki Y, Kasahara A, et al. Linearity, bias, intrascanner repeatability, and interscanner reproducibility of quantitative multidynamic multiecho sequence for rapid simultaneous relaxometry at 3 T: a validation study with a standardized phantom and healthy controls. Invest Radiol 2019;54(1):39–47.
[15] Hagiwara A, Warntjes M, Hori M, Andica C, Nakazawa M, Kumamaru KK, et al. SyMRI of the brain: rapid quantification of relaxation rates and proton density, with synthetic MRI, automatic brain segmentation, and myelin measurement. Invest Radiol 2017;52(10):647–57.
[16] Tanenbaum LN, Tsiouris AJ, Johnson AN, Naidich TP, DeLano MC, Melhem ER, et al. Synthetic MRI for clinical neuroimaging: results of the magnetic resonance image compilation (MAGiC) prospective, multicenter, multireader trial. AJNR Am J Neuroradiol 2017;38(6):1103–10.
[17] Blystad I, Warntjes JB, Smedby O, Landtblom AM, Lundberg P, Larsson EM. Synthetic MRI of the brain in a clinical setting. Acta Radiol 2012;53(10):1158–63.
[18] Warntjes M, Engstrom M, Tisell A, Lundberg P. Modeling the presence of myelin and edema in the brain based on multi-parametric quantitative MRI. Front Neurol 2016;7:16.
[19] West J, Warntjes JB, Lundberg P. Novel whole brain segmentation and volume estimation using quantitative MRI. Eur Radiol 2012;22(5):998–1007.
[20] Hagiwara A, Hori M, Yokoyama K, Takemura MY, Andica C, Tabata T, et al. Synthetic MRI in the detection of multiple sclerosis plaques. AJNR Am J Neuroradiol 2017;38(2):257–63.
[21] Granberg T, Uppman M, Hashim F, Cananau C, Nordin LE, Shams S, et al. Clinical feasibility of synthetic MRI in multiple sclerosis: a diagnostic and volumetric validation study. AJNR Am J Neuroradiol 2016;37(6):1023–9.
[22] Wallaert L, Hagiwara A, Andica C, Hori M, Yamashiro K, Koshino S, et al. The advantage of synthetic MRI for the visualization of anterior temporal pole lesions on double inversion recovery (DIR), phase-sensitive inversion recovery (PSIR), and myelin images in a patient with CADASIL. Magn Reson Med Sci 2018;17(4):275–6.
[23] Andica C, Hagiwara A, Nakazawa M, Kumamaru KK, Hori M, Ikeno M, et al. Synthetic MR imaging in the diagnosis of bacterial meningitis. Magn Reson Med Sci 2017;16(2):91–2.
[24] Kvernby S, Warntjes MJ, Haraldsson H, Carlhall CJ, Engvall J, Ebbers T. Simultaneous three-dimensional myocardial T1 and T2 mapping in one breath hold with 3D-QALAS. J Cardiovasc Magn Reson 2014;16:102.
[25] Kvernby S, Warntjes M, Engvall J, Carlhall CJ, Ebbers T. Clinical feasibility of 3D-QALAS - single breath-hold 3D myocardial T1- and T2-mapping. Magn Reson Imaging 2017;38:13–20.
[26] Fujita S, Hagiwara A, Hori M, Warntjes M, Kamagata K, Fukunaga I, et al. 3D quantitative synthetic MRI-derived cortical thickness and subcortical brain volumes: scan–rescan repeatability and comparison with conventional T1 -weighted images. J Magn Reson Imaging 2019. (Epub ahead of print).
[27] Russek SBM, Jackson E, et al. Characterization of NIST/ISMRM MRI system phantom. Proceedings of the 20th annual meeting of ISMRM Melbourne, Victoria, Australia. 2456. 2012.
[28] Keenan KSK, Boss M, et al. Multi-site, multi-vendor comparison of T1 measurement using ISMRM/NIST system phantom. Proceedings of the 24th annual meeting of ISMRM. 3290. 2016.
[29] User manual, version 8.0.0, SyMRI 8. Linko¨ping: SyntheticMR AB. 2016.
[30] Mazziotta J, Toga A, Evans A, Fox P, Lancaster J, Zilles K, et al. A probabilistic atlas and reference system for the human brain: International Consortium for Brain Mapping (ICBM). Philos Trans R Soc Lond B Biol Sci 2001;356(1412):1293–322.
[31] Mazziotta J, Toga A, Evans A, Fox P, Lancaster J, Zilles K, et al. A four-dimensional probabilistic atlas of the human brain. J Am Med Inform Assoc 2001;8(5):401–30.
[32] Maintz JB, Viergever MA. A survey of medical image registration. Med Image Anal 1998;2(1):1–36.
[33] Neeb H, Zilles K, Shah NJ. A new method for fast quantitative mapping of absolute water content in vivo. Neuroimage 2006;31(3):1156–68.
[34] McKenzie CA, Chen Z, Drost DJ, Prato FS. Fast acquisition of quantitative T2 maps. Magn Reson Med 1999;41(1):208–12.
[35] Deichmann R. Fast high-resolution T1 mapping of the human brain. Magn Reson Med 2005;54(1):20–7.
[36] Whittall KP, MacKay AL, Graeb DA, Nugent RA, Li DK, Paty DW. In vivo measurement of T2 distributions and water contents in normal human brain. Magn Reson Med 1997;37(1):34–43.
[37] Oh J, Cha S, Aiken AH, Han ET, Crane JC, Stainsby JA, et al. Quantitative apparent diffusion coefficients and T2 relaxation times in characterizing contrast enhancing brain tumors and regions of peritumoral edema. J Magn Reson Imaging 2005;21(6):701–8.
[38] Ernst T, Kreis R, Ross BD. Absolute quantitation of water and metabolites in the human brain. I. Compartments and water. J Magn Reson 1993;102(1):1–8.
[39] West J, Aalto A, Tisell A, Leinhard OD, Landtblom AM, Smedby O, et al. Normal appearing and diffusely abnormal white matter in patients with multiple sclerosis assessed with quantitative MR. PLoS One 2014;9(4):e95161.
[40] Hagiwara A, Hori M, Yokoyama K, Takemura MY, Andica C, Kumamaru KK, et al. Utility of a multiparametric quantitative MRI model that assesses myelin and edema for evaluating plaques, periplaque white matter, and normal-appearing white matter in patients with multiple sclerosis: a feasibility study. AJNR Am J Neuroradiol 2017;38(2):237–42.
[41] Wang H, Yuan H, Shu L, Xie J, Zhang D. Prolongation of T(2) relaxation times of hippocampus and amygdala in Alzheimer's disease. Neurosci Lett 2004;363(2):150–3.
[42] Just M, Thelen M. Tissue characterization with T1, T2, and proton density values: results in 160 patients with brain tumors. Radiology 1988;169(3):779–85.
[43] Lustig M, Donoho D, Pauly JM. Sparse MRI: the application of compressed sensing for rapid MR imaging. Magn Reson Med 2007;58(6):1182–95.